Positron emission tomography with computed tomography imaging of neuroinflammation in experimental autoimmune encephalomyelitis

Caius G. Radu*, Chengyi J. Shu†, Stephanie M. Shelly*, Michael E. Phelps*‡, and Owen N. Witte*†‡§¶‖

Departments of *Molecular and Medical Pharmacology and †Microbiology, Immunology, and Molecular Genetics, David Geffen School of Medicine, ‡Institute for Molecular Medicine, §Institute for Stem Cell Biology and Medicine, and ¶Howard Hughes Medical Institute, University of California, Los Angeles, CA 90095

Contributed by Owen N. Witte, November 28, 2006 (sent for review November 6, 2006)

2-[^{18}F]Fluoro-2-deoxy-D-glucose positron emission tomography ([^{18}F]FDG PET) detection of the up-regulated glycolysis associated with malignant transformation is a noninvasive imaging technique used extensively in cancer diagnosis. Although striking similarities exist in glucose transport and metabolism between tumor cells and activated immune cells, the potential use of [^{18}F]FDG PET for the diagnosis and evaluation of autoimmune disorders has not been systematically investigated. Here we ask whether [^{18}F]FDG PET in conjunction with computed tomography (CT) could be used to monitor a complex autoimmune disorder such as murine experimental autoimmune encephalomyelitis (EAE) and whether this approach is sensitive enough to evaluate therapeutic interventions. We found that (*i*) coregistration of metabolic (i.e., microPET) and high-resolution anatomical (i.e., CT) images allows serial quantification of glycolysis with [^{18}F]FDG in various spinal column segments; (*ii*) [^{18}F]FDG PET/CT can detect the increased glycolysis associated with paralysis-causing inflammatory infiltrates in the spinal cord; and (*iii*) the [^{18}F]FDG measure of glycolysis in the spinal cord is sensitive to systemic immunosuppressive therapy. These results highlight the potential use of serial [^{18}F]FDG PET/CT imaging to monitor neuroinflammation in EAE and suggest that similar approaches could be applied to the diagnosis and evaluation of other autoimmune and inflammatory disorders in animal models and in humans.

2-[^{18}F]fluoro-2-deoxy-D-glucose | glycolysis | activated T lymphocytes

Many decades ago, the German biochemist Otto Warburg observed that, in contrast to normal cells, cancer cells metabolize glucose to lactate even in the presence of oxygen (1). Because glycolysis produces only 2 molecules of ATP per molecule of glucose, compared with 36 molecules of ATP in the Krebs cycle, the glycolytic rate of cancer cells is amplified to meet their energy needs. Cancer cells further amplify glycolysis through activation of the hexose monophosphate shunt in which glucose is used to provide the carbon backbone for DNA and RNA synthesis (2). Warburg's findings represent the basis of a modern, widely used cancer diagnostic method using positron emission tomography (PET) and the glucose analog 2-[^{18}F]fluoro-2-deoxy-D-glucose ([^{18}F]FDG) for imaging and measuring glycolysis (3–6). Although accelerated glycolysis is a hallmark of cancer, recent research has demonstrated that this process is not unique to tumor cells. In T cells, similar metabolic changes occur that rapidly hyperinduce glycolysis within 1 h of stimulation (7–9). Moreover, a significant overlap is known to exist between activated T cells and cancer cells in terms of signaling events leading to up-regulated aerobic glycolysis. Key players include AKT, which is activated by phosphatidylinositol 3-kinase (10), and the PIM1 and PIM2 kinases, which are activated by the Janus kinase and signal transducer and activator of transcription pathway (10). In addition to that in T cells, elevated glycolysis after activation has been reported in other immune cell types such as macrophages (11) and neutrophils (12).

Despite these striking metabolic similarities between tumor cells and activated immune cells, the value of [^{18}F]FDG PET for the diagnosis and evaluation of autoimmune and inflammatory disorders remains to be determined. It is possible that, compared with malignant tumors, inflammatory infiltrates might be more difficult to image by [^{18}F]FDG PET because they are more heterogeneous in terms of cellular composition, are more diffuse topographically, and often contain smaller numbers of cells. However, several lines of evidence indicate that imaging inflammatory responses with [^{18}F]FDG PET is feasible. First, it is well known that sites of inflammation are often mistakenly identified as malignant tumors by [^{18}F]FDG PET (reviewed in ref. 13). Second, we recently showed that in mice [^{18}F]FDG PET can be used to visualize lymphocyte activation in local draining lymph nodes during an antitumor immune response (14). Third, examples of using [^{18}F]FDG PET to evaluate abnormal glycolysis in autoimmune disorders such as rheumatoid arthritis (15–17) and systemic lupus erythematosus (SLE) (18) can be found in the literature, albeit in much lower numbers relative to cancer studies.

A general limitation of metabolic PET imaging is the relatively low (≈1–2 mm) spatial resolution of existing scanners for rodents (19). Thus, it is sometimes difficult to precisely determine the exact anatomical location of glycolysis within PET images (16). This drawback can be minimized by the merger of PET and computed tomography (CT) imaging (20). We therefore reasoned that nearly simultaneous acquisition of metabolic PET images and high-resolution (50–200 μm) morphological CT images (19) should allow improved anatomical localization of [^{18}F]FDG measures of glycolysis at sites affected by the presence of inflammatory infiltrates. To test this possibility and investigate the value of PET metabolic imaging in a typical autoimmune disorder, we used [^{18}F]FDG PET/CT to monitor disease progression and therapeutic responses in murine experimental autoimmune encephalomyelitis (EAE). The selection of this animal model was motivated by multiple reasons including the widely accepted view of EAE as "the" prototypic organ-specific autoimmune disorder (21), as well as its similarities to the human disease multiple sclerosis (MS) (22). Most importantly, clinical

Author contributions: C.G.R. and C.J.S. contributed equally to this work; C.G.R., C.J.S., M.E.P., and O.N.W. designed research; C.G.R., C.J.S., and S.M.S. performed research; C.G.R., C.J.S., and S.M.S. analyzed data; and C.G.R. wrote the paper.

The authors declare no conflict of interest.

Freely available online through the PNAS open access option.

Abbreviations: PET, positron emission tomography; [^{18}F]FDG, 2-[^{18}F]fluoro-2-deoxy-D-glucose; CT, computed tomography; EAE, experimental autoimmune encephalomyelitis; MOG, myelin oligodendrocyte glycoprotein; CFA, complete Freund's adjuvant; PTX, pertussis toxin; ROI, region of interest; ^{14}C-DG, ^{14}C-labeled 2-deoxy-D-glucose; DEX, dexamethasone; MS, multiple sclerosis.

‖To whom correspondence should be addressed at: Howard Hughes Medical Institute, University of California at Los Angeles, 675 Charles E. Young Drive South, 5-748 MRL Building, Los Angeles, CA 90095-1662. E-mail: owenw@microbio.ucla.edu.

manifestations in the EAE model are easy to recognize and are the consequence of pathogenic T cell infiltrations in the white matter of the central nervous system (CNS). In the spinal cord, such cellular infiltrates develop in an otherwise "lymphocyte-free" zone after well defined temporal kinetics. Taken together, these unique features of the EAE model should simplify the microPET/CT detection, localization, and quantification of the glycolytic changes associated with immune activation.

It is important to note that, before our study, several groups used PET to image disease progression in EAE. Reported approaches include the following: (*i*) the use of a positron-labeled inducible nitric oxide synthetase inhibitor (23), (*ii*) imaging microglial activation by using the ^{11}C-labeled isoquinoline (*R*)-PK 11195 (24–26), and, more recently, (*iii*) the use of ^{11}C-labeled 1,4-bis(*p*-aminostyryl)-2-methoxy benzene as a myelin-specific tracer to monitor demyelinating lesions (27). In contrast to these studies, our approach was based on the use of a Food and Drug Administration-approved PET probe [^{18}F]FDG, which is routinely used in clinical practice. We show that, in combination with CT, [^{18}F]FDG PET can be used for serial *in vivo* noninvasive measurements of glycolysis in the spinal cord. Quantification of the [^{18}F]FDG PET images showed that increases in glycolysis correlated with the onset of EAE neurological symptomatology and with the presence of inflammatory infiltrates detected by histological examination. Moreover, our results suggest that [^{18}F]FDG PET/CT imaging is sensitive to the effects of systemic immunosuppressive therapy on local changes in glucose metabolism induced by inflammation.

Results

EAE as a Model System to Evaluate the Use of [^{18}F]FDG PET/CT in Hyperactive Immune Disorders. In the C57BL/6 strain of mice, EAE has been induced via a single administration of an immunodominant epitope of myelin oligodendrocyte glycoprotein ($MOG_{35–55}$) emulsified in complete Freund's adjuvant (CFA) (28). Similar to most other murine models of EAE, disease induction in C57BL/6 mice also requires the use of pertussis toxin (PTX). Although the prevailing dogma is that PTX facilitates the access of activated T cells to the CNS by helping them to cross the blood–brain barrier (29), the molecular mechanisms of this process are complex. According to a recent study (30), PTX alone can induce the recruitment of leukocytes and activated T cells to the CNS via a Toll-like receptor 4 (TLR4)-dependent pathway. The requirement of PTX for EAE induction was clearly reflected by the disease incidence observed in the current study (Fig. 1). Thus, 39 of the 42 mice immunized with $MOG_{35–55}$/CFA/PTX developed EAE, with an average clinical score of 2.5.

To determine whether quantification of glycolysis in the spinal cord when using [^{18}F]FDG can be correlated with clinical signs of EAE, mice were serially imaged by microPET/CT from day 8 to 21 after immunization. [^{18}F]FDG microPET and CT images acquired in the same session were merged as shown in Fig. 2*A* by using a previously described approach (31). The CT scan allowed us to draw regions of interest (ROIs) shaped as elliptical cylinders over each vertebra (Fig. 2*A*). The [^{18}F]FDG signal was quantified by using AMIDE software (32) and normalizing the sum of the vertebral ROIs percent injected dose (%ID) per gram of tissue over the total amount of radioactivity in the whole body of the mouse, excluding the amount trapped in the tail (Fig. 2*B*).

EAE-Affected Mice Show Higher Uptake of [^{18}F]FDG in the Spinal Column. We determined whether inflammation-induced changes in glycolysis in the spinal cord of EAE-affected mice could be detected and quantified by [^{18}F]FDG PET/CT imaging. Fig. 3*A* shows a comparison of the [^{18}F]FDG PET/CT scans of a $MOG_{35–55}$/CFA/PTX-immunized mouse and of a nonimmunized mouse. The immunized mouse was scanned 2 days before

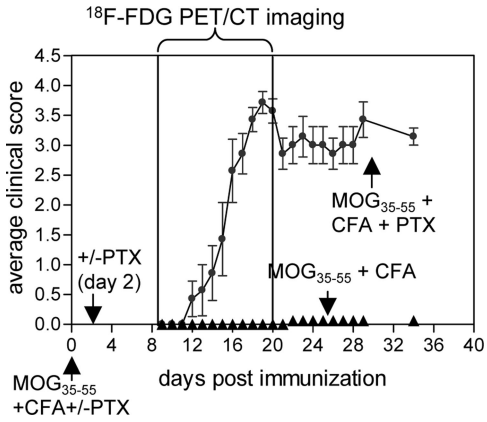

Fig. 1. Clinical and PET/CT evaluation of EAE. Typical clinical scores for C57BL/6 mice immunized with $MOG_{35–55}$/CFA and treated with PTX on days 0 and 2 ($n = 7$). Results shown are representative of five independent experiments, each with four to eight mice per group. Mice were serially imaged by using [^{18}F]FDG PET/CT between days 8 and 21 after immunization.

disease onset and at three subsequent time points characterized by different clinical scores. An increase in glycolysis was observed in the diseased mouse at anatomical locations consistent with the presence of inflammatory infiltrates in the spinal cord.

A caveat of this animal model is that disease induction requires the use of a strong adjuvant, CFA. It is conceivable that CFA-induced activation of innate immune pathways could have resulted in systemic alterations in glucose metabolism unrelated to the inflammatory infiltrates affecting the CNS. To determine whether we were in fact imaging autoimmunity rather than nonspecific adjuvant-driven activation of the innate immune system, we also scanned mice that were immunized with antigen and adjuvant but were not treated with PTX. Whereas these mice mounted a strong response in the periphery against the immunizing $MOG_{35–55}$ antigen, EAE incidence was greatly reduced in this experimental group (only 3 of 47 mice developed mild EAE, with a clinical score of 1). The differential rate of glycolysis in EAE-affected mice (score of ≥1 on days 14–17) relative to that in nonimmunized mice and mice immunized with $MOG_{35–55}$/CFA only, without PTX treatment, is shown in Fig. 3*B*. A significant increase in glycolysis in all three major spinal

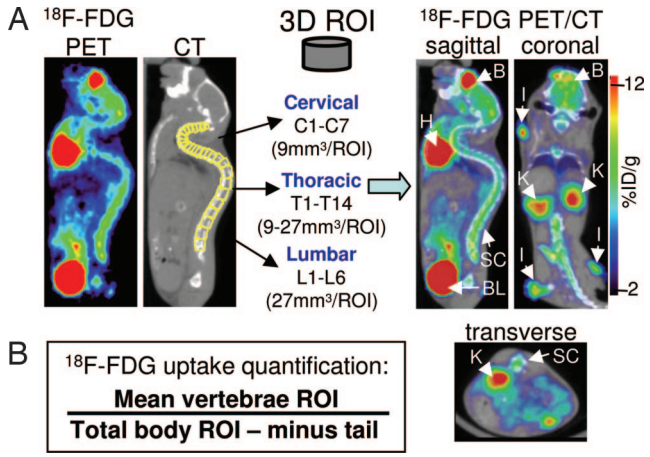

Fig. 2. Data analysis. (*A*) Fusion of microPET and microCT images recorded in the same session and drawing of 3D ROIs corresponding to each vertebra. B, brain; H, heart; SC, spinal column; BL, bladder; K, kidney; I, immunization site; %ID/g, percent injected dose per gram of tissue. (*B*) Formula to quantify glycolysis.

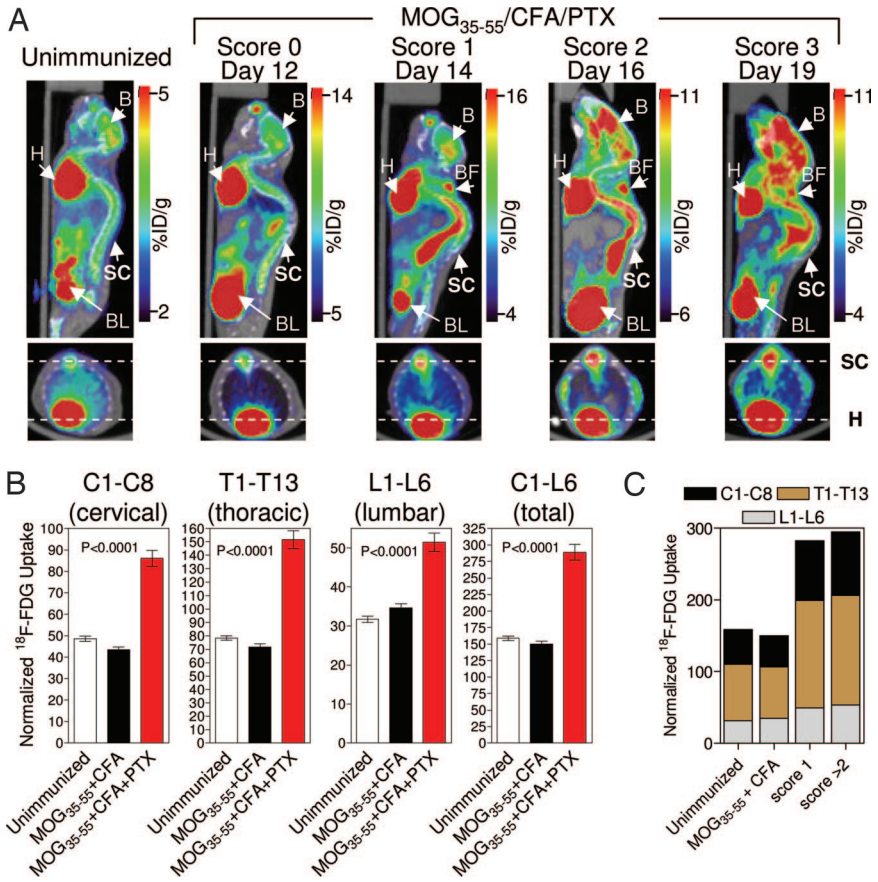

Fig. 3. Increased glycolysis at anatomical locations corresponding to the spinal cord/column in EAE-affected mice. (*A*) [^{18}F]FDG PET/CT scans (coronal and transverse sections) of an nonimmunized mouse and of a MOG_{35-55}/CFA/PTX-immunized mouse at various time points before and after EAE onset. B, brain; H, heart; SC, spinal column; BL, bladder; BF, brown fat. (*B*) Elevated glycolysis in the cervical, thoracic, and lumbar spinal column segments of EAE-affected mice, as well as in the entire (C1–L6) spinal column. Numbers of mice were as follows: nonimmunized group, $n = 8$; MOG_{35-55}/CFA-immunized group, $n = 11$; and MOG_{35-55}/CFA/PTX-immunized group, $n = 18$. Mice were imaged between days 13 and 21 after immunization in four independent experiments. (*C*) Glycolysis in the spinal column does not reflect disease severity measured by using the clinical score. Numbers of mice per data point were as follows: nonimmunized, $n = 8$; score of 1, $n = 8$; and score of ≥ 2, $n = 10$.

column segments (i.e., cervical, thoracic, and lumbar) was detected only in the EAE-affected, MOG_{35-55}/CFA/PTX-immunized mice. These results suggest that the alterations in glycolysis seen in the PET images were the reflection of the disease process itself rather than an artifact of the immunization protocol.

Although increases in glycolysis were reproducibly detected in mice with mild signs of EAE (score of 1, Fig. 3*C*), PET scans performed 2 days before the onset of clinical symptoms failed to detect any differences among the three experimental groups (data not shown). Furthermore, the rates of glycolysis observed in the spinal column were not correlated with the severity of the disease as measured by the clinical score (Fig. 3*C*).

^{14}C-Labeled 2-Deoxy-D-Glucose (^{14}C-DG) Autoradiography of Isolated Spinal Cords Correlates with *in Vivo* [^{18}F]FDG Measurements. Although CT coregistration of anatomical images greatly improved our ability to localize and quantify glycolysis as measured with [^{18}F]FDG, we could not unequivocally pinpoint the anatomical location of these metabolic changes. In addition to inflammatory infiltrates in the spinal cord, other sources of increased glycolysis could potentially include immunization-induced metabolic changes in the bone marrow of the vertebrae, in the bone itself, or in anatomical structures located in close proximity to the spinal column (e.g., lymph nodes or other soft tissues such as muscle). To determine the contribution of spinal cord inflammatory infiltrates to the changes in glycolysis imaged with PET, we performed independent measurement of glycolysis using autoradiography with ^{14}C-DG of isolated organs. EAE-affected (MOG_{35-55}/CFA/PTX-immunized) and control (MOG_{35-55}/CFA-immunized) mice were i.v. injected with ^{14}C-DG, an analogue of glucose with chemical and physiological properties very similar to those of [^{18}F]FDG (33). After an uptake time of 1–2 h *in vivo*, spinal cords were isolated and sectioned for autoradiography. As shown in Fig. 4*A*, we observed increased localization of ^{14}C-DG as a measure of glycolysis in spinal cords isolated from EAE-affected mice. As predicted by [^{18}F]FDG PET/CT imaging (Fig. 3*B*), no localization from the autoradiographic study was observed in spinal cords isolated from disease-free mice immunized with antigen and adjuvant but not treated with PTX. These *ex vivo* results correlated well with our histological examination of the inflammatory infiltrates (Fig. 4*B*) and also confirmed an observation made by using ^{14}C-DG autoradiography >2 decades ago regarding the increased glycolysis associated with inflammatory CNS lesions in EAE (34).

[^{18}F]FDG PET Identifies Reductions in Inflammatory-Induced Increases in Glycolysis in the Spinal Column due to Systemic Immunosuppressive Treatment. To further investigate the potential use of [^{18}F]FDG PET/CT in EAE, we sought to determine whether this technique could be used to monitor the effects of systemic immunosup-

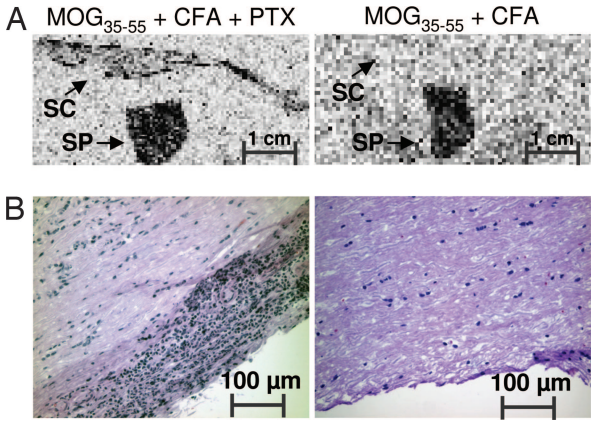

Fig. 4. *Ex vivo* analyses of glycolysis and of inflammatory infiltrates in the spinal cord. (*A*) Glycolysis imaged with ^{14}C-DG autoradiography. Although glycolysis was detected only in spinal cords isolated from mice immunized with $MOG_{35–55}$/CFA/PTX, glycolysis in the spleen was independent of the PTX treatment. SC, spinal cord; SP, spleen. (*B*) H&E staining of the spinal cord indicating the presence of inflammatory infiltrates in mice treated with PTX. These results are representative of three independent experiments.

pressive therapies known to block the development of neurological manifestations in this animal model. Given the critical role of $CD4^+$ T cells in EAE pathogenesis and the likely possibility that increases in glycolysis in the spinal cord reflected the accumulation of activated T lymphocytes, we used dexamethasone (DEX), a drug known to exert pleiotropic and potent immunosuppressive effects on T cells (35). Moreover, DEX has been previously shown to completely block EAE development in rodents (36).

Mice were scanned before (days 6–14) and after (days 15–21) the average day of EAE onset. We compared mice immunized with $MOG_{35–55}$/CFA (which did not develop EAE) with mice immunized with $MOG_{35–55}$/CFA/PTX that were either treated with DEX or left untreated (Fig. 5). Between days 15 and 21, glycolysis was clearly increased only in those mice immunized with $MOG_{35–55}$/CFA/PTX that were left untreated with DEX (Fig. 5 *B* and *C*). This increase was correlated with the onset of neurological manifestations as shown in Fig. 3. We also observed an intriguing temporal pattern of glycolytic alterations. In both untreated mice and DEX-treated mice that were immunized with $MOG_{35–55}$/CFA/PTX, scans performed between days 6 and 8 after immunization showed consistent and significant increases in glycolysis at anatomical locations corresponding to the spinal cord or to immediately adjacent tissues (Fig. 5 *A* and *C*). It is important to note that, on average, these time points preceded EAE onset by 7 days. The most likely interpretation of this result was that the early (days 6–8) increases in glycolysis reflected the activation of the innate immune system by PTX. Such effects were insensitive to DEX treatment and might be explained by the PTX-mediated activation of a TLR4-dependent mechanism, such as that proposed by Kerfoot *et al.* (30). In contrast, increases in glycolysis at later time points (days 15–21) most probably reflected the DEX-sensitive, antigen-dependent activation of the adaptive arm of the immune system. The results shown in Fig. 5*C* further support this interpretation. Quantitation of glycolysis in mice treated with PTX alone showed increased glycolysis localized in the spinal cord or in its immediate proximity (Fig. 5*C*). The PTX-induced effects were transient, and no differences

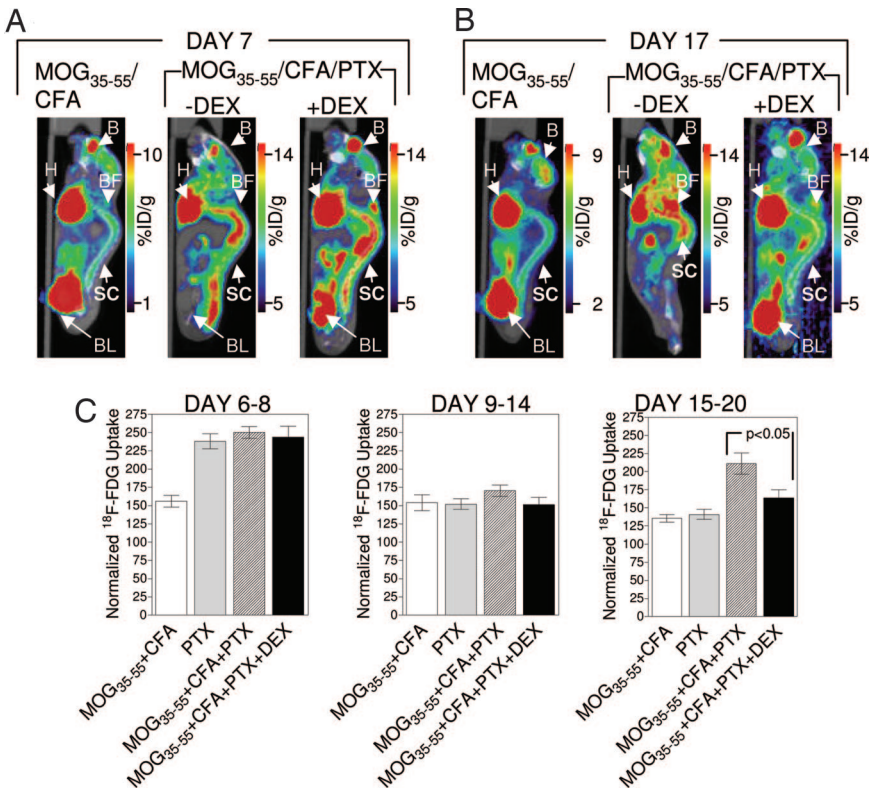

Fig. 5. Systemic immunosuppressive treatment of $MOG_{35–55}$/CFA/PTX-immunized mice with DEX significantly reduced glycolysis, as imaged with [^{18}F]FDG. (*A* and *B*) Representative [^{18}F]FDG PET/CT scans of mice immunized with $MOG_{35–55}$/CFA and of mice immunized with $MOG_{35–55}$/CFA/PTX, treated or not with DEX. Mice were imaged on days 7 (*A*) and 17 (*B*) after immunization. Before onset (day 7), changes in glycolysis were not sensitive to DEX treatment. (*C*) PTX alone can induce transient changes in glycolysis. Numbers of mice were as follows: $MOG_{35–55}$/CFA-immunized group, $n = 14$; PTX-immunized group, $n = 5$; $MOG_{35–55}$/CFA/PTX-immunized group untreated with DEX, $n = 20$; and $MOG_{35–55}$/CFA/PTX-immunized group treated with DEX, $n = 11$.

in glycolysis among experimental groups were observed during the intermediate time frame (days 9–14).

Discussion

Advantages and Limitations of [^{18}F]FDG PET/CT Imaging of EAE. The initial question that motivated our study was to determine whether molecular imaging with PET using the widely available probe [^{18}F]FDG, combined with anatomical (i.e., CT) imaging, would prove useful in monitoring a complex autoimmune disorder such as EAE. Our results support an affirmative answer to this question. First, coregistration of anatomical structures using CT was extremely useful for localizing and analyzing PET images of glycolysis. Second, [^{18}F]FDG PET/CT detected changes in glucose metabolism at anatomical locations consistent with the presence of inflammatory infiltrates in the spinal cord. These changes were reproducibly detected in mice with minimal neurological symptomatology (clinical score of 1), and they coincided with the onset of the disease. Third, alterations in glucose metabolism revealed by [^{18}F]FDG PET/CT imaging were sensitive to immunosuppressive therapy with DEX.

The current study encountered some of the limitations of [^{18}F]FDG PET/CT imaging in EAE that need to be considered for future applications. Although [^{18}F]FDG PET/CT can detect metabolic changes induced by PTX that precede the onset of neurological manifestations, the relationship between these alterations and the biological mechanisms of autoimmune demyelination needs to be further investigated. The question of whether this imaging technology can be used to "predict" disease onset might be better answered by using recently created mouse EAE models characterized by spontaneous development of autoimmune demyelination (37, 38). Moreover, we were unable to correlate glycolysis imaged with [^{18}F]FDG PET with disease severity as represented by the clinical score. This could reflect current limitations of PET technology in terms of sensitivity. Alternatively, these findings might be related to divergent effects of the disease process on the glucose metabolism in the spinal cord. Thus, in mice with advanced disease, areas of hypermetabolism due to inflammatory infiltrates in the white matter could coexist with adjacent areas of hypometabolism due to gray matter pathology.

Potential Use of [^{18}F]FDG PET/CT in MS. Our results also raise the question of whether this imaging modality can be of value in monitoring the presence of inflammatory infiltrates in the human autoimmune demyelinating disorder MS. Several [^{18}F]FDG PET imaging studies on MS have been published during the last 15 years (39–45). Interestingly, however, the goal of these studies was not to detect and monitor inflammation but rather to determine whether the regional cerebral metabolic rate of glucose (rCMRGlc) estimated by using [^{18}F]FDG PET can be used as an indirect measurement of cortical impairment in MS. Overall, these studies (39–45) detected mild global and regional (i.e., frontal cortex, basal ganglia, hippocampal, and thalamic) reductions in rCMRGlc. The interpretation of [^{18}F]FDG PET data from these studies (39–45) might be further complicated by the existence of several clinical forms of MS including acute MS, relapsing remitting MS, secondary progressive MS, and primary progressive MS. Recent histological data suggest that MS starts as a focal inflammatory disease that slowly becomes compartmentalized in the CNS, giving rise to widespread diffuse neurodegeneration characterized by axonal injury in the white matter and cortical demyelination (46). Therefore, studies using [^{18}F]FDG PET might prove more informative in the early, and pathologically focal, inflammatory stages of the disease when [^{18}F]FDG PET can be used to complement magnetic resonance imaging (MRI), a technique known to lack histological specificity. Moreover, we would like to suggest that, as for MRI studies (47), [^{18}F]FDG PET studies of glucose metabolism in MS patients should not be limited to the brain but should also include imaging of the spinal cord, a common site of demyelinating lesions.

Metabolic PET Imaging as an *in Vivo* Measurement of Immune Activation. Our results in the EAE model suggest potential uses for [^{18}F]FDG PET/CT in the diagnosis and monitoring of other disorders characterized by hyperactive immunity. In a broader sense, they also make a case for using PET to measure other metabolic pathways as functional readouts of immune activation. Thus, fatty acids and amino acids are also used by lymphocytes as sources of energy (10), and, similar to glucose, their utilization is sensitive to immune activation. For example, changes in amino acid transport in activated T cells are reflected in the up-regulated surface expression of the CD98 surface antigen also known as the 4F2 heavy-chain component (4F2hc). This molecule is induced by CD28 costimulation in a rapamycin-sensitive fashion (48) and, as a heterodimer with the L system amino acid transporter 1 light chain, participates in the transport of large neutral amino acids. It is therefore likely that identification of novel molecular PET probes specific for major metabolic pathways modulated by immune activation could greatly expand our ability to noninvasively monitor the ongoing biology of immune responses under physiological and pathological conditions.

Materials and Methods

Mice. C57BL/6 mice were bred and maintained according to the guidelines of the Department of Laboratory Animal Medicine (DLAM) at the University of California, Los Angeles. EAE-inducing immunizations were carried out by using DLAM-approved protocols.

EAE Induction, Clinical Scoring, and DEX Treatment. Female mice (7–10 weeks old) were immunized s.c. with 100 μg of $MOG_{35–55}$ (MEVGWYRSPFSRVVHLYRNGK, synthesized by C S Bio Company, Menlo Park, CA) in an emulsion of incomplete Freund's adjuvant (F5506; Sigma, St. Louis, MO) and lyophilized heat-inactivated *Mycobacterium tuberculosis* (100 μg per mouse, lot no. 3114-33, strain H37Ra; Difco, Detroit, MI) distributed on four sites on the back. Mice were injected i.p. with 200 ng of PTX (516561, Calbiochem, Darmstadt, Germany) in PBS on days 0 and 2. Mice were scored for the severity of the disease by using the following scale: 0, no abnormality; 1, limp tail; 2, mild hind limb weakness; 3, severe hind limb weakness; 4, complete hind limb paralysis; 5, quadriplegia or premoribound state. For DEX treatment, mice received daily i.p. injections starting on day 3 after immunization with 10 mg/kg drug (D1756; Sigma) dissolved in 200 μl of PBS.

MicroPET/CT Imaging. Animals were anesthetized with 2% isoflurane, injected i.v. with [^{18}F]FDG, and scanned by using a Focus 220 microPET scanner (Siemens, Knoxville, TN) as described (14). Images were reconstructed by using an iterative maximum *a posteriori* algorithm (49). In the same imaging session, CT images were also acquired by using a MicroCAT II instrument (Siemens). Vertebral ROIs were drawn to correspond to the following dimensions: the lumbar (L) segment L1–L6 and the thoracic (T) segment T12–T13 − $3 \times 3 \times 3$ mm^3; T10–T11 − $3 \times 3 \times 2$ mm^3; T9 − $3 \times 3 \times 1.5$ mm^3; T6–T8 − $3 \times 3 \times 1.25$ mm^3; and T1–T5 and the cervical (C) segment C1–C8 − $3 \times 3 \times 1$ mm^3.

Autoradiography and Histology. Mice were anesthetized with 2% isoflurane and injected i.v. with 1 μCi (1 Ci = 37 GBq) of [^{14}C]-2-deoxyglucose (D6784; Sigma) in PBS. After 1–2 h, mice were killed and subjected to whole-body perfusion with PBS and 4% paraformaldehyde. Spinal cords and spleens were harvested and embedded in OCT compound (Sakura Finetek, Torrance,

CA). Frozen sections (18 μm) were developed for 3 weeks by using BAS-TR2025 imaging screens (FujiFilm Life Science, Stamford, CT) and visualized by using a BAS-5000 phosphor imager (FujiFilm Life Science). Frozen sections (4 μm) were used for H&E staining of inflammatory infiltrates.

Data Analysis. Graphs were constructed by using PRISM software (version 4.02; GraphPad, San Diego, CA). Data are presented as mean ± SE.

We thank Dr. Waldemar Ladno and Judy Edwards for assistance with PET/CT imaging, Dr. Satyamurthy and the cyclotron staff for the production of [^{18}F]FDG, David Stout for technical advice, Dr. Arion Chatziioannou for helpful suggestions, Shirley Quan and Lakeisha Perkins for outstanding technical assistance, Andrew Tran for help with data analysis, and Barbara Anderson for help with preparation of the manuscript. O.N.W. is an investigator of the Howard Hughes Medical Institute. C.G.R. was supported by *In Vivo* Cellular and Molecular Imaging Centers (ICMIC) Developmental Project Award NIH P50 CA86306 from the National Cancer Institute, National Institutes of Health. C.G.R. acknowledges unrestricted support from Merck Research Laboratories. C.J.S. was supported by National Institutes of Health Research Training in Pharmacological Sciences Training Grant PHS T32 CM008652. This research was supported in part by U.S. Department of Energy Contract DE-FG02-06ER64249 and by National Cancer Institute Grant R24CA92865.

1. Warburg O (1956) *Science* 123:309–314.
2. Gatenby RA, Gillies RJ (2004) *Nat Rev Cancer* 4:891–899.
3. Silverman DH, Hoh CK, Seltzer MA, Schiepers C, Cuan GS, Gambhir SS, Zheng L, Czernin J, Phelps ME (1998) *Semin Radiat Oncol* 8:183–196.
4. Gambhir SS, Czernin J, Schwimmer J, Silverman DH, Coleman RE, Phelps ME (2001) *J Nucl Med* 42:1S–93S.
5. Czernin J, Phelps ME (2002) *Annu Rev Med* 53:89–112.
6. Czernin J, Weber WA, Herschman HR (2006) *Annu Rev Med* 57:99–118.
7. Frauwirth KA, Riley JL, Harris MH, Parry RV, Rathmell JC, Plas DR, Elstrom RL, June CH, Thompson CB (2002) *Immunity* 16:769–777.
8. Frauwirth KA, Thompson CB (2004) *J Immunol* 172:4661–4665.
9. Greiner EF, Guppy M, Brand K (1994) *J Biol Chem* 269:31484–31490.
10. Fox CJ, Hammerman PS, Thompson CB (2005) *Nat Rev Immunol* 5:844–852.
11. Gamelli RL, Liu H, He LK, Hofmann CA (1994) *Shock* 1:395–400.
12. Chen DL, Schuster DP (2004) *Am J Physiol* 286:L834–L840.
13. Strauss LG (1996) *Eur J Nucl Med* 23:1409–1415.
14. Shu CJ, Guo S, Kim YJ, Shelly SM, Nijagal A, Ray P, Gambhir SS, Radu CG, Witte ON (2005) *Proc Natl Acad Sci USA* 102:17412–17417.
15. Beckers C, Jeukens X, Ribbens C, Andre B, Marcelis S, Leclercq P, Kaiser MJ, Foidart J, Hustinx R, Malaise MG (2006) *Eur J Nucl Med Mol Imaging* 33:275–280.
16. Beckers C, Ribbens C, Andre B, Marcelis S, Kaye O, Mathy L, Kaiser MJ, Hustinx R, Foidart J, Malaise MG (2004) *J Nucl Med* 45:956–964.
17. Peterfy CG (2003) *Curr Opin Rheumatol* 15:288–295.
18. Peterson PL, Axford JS, Isenberg D (2005) *Best Pract Res Clin Rheumatol* 19:727–739.
19. Massoud TF, Gambhir SS (2003) *Genes Dev* 17:545–580.
20. Tsukamoto E, Ochi S (2006) *Ann Nucl Med* 20:255–267.
21. Zamvil SS, Steinman L (1990) *Annu Rev Immunol* 8:579–621.
22. Steinman L, Zamvil SS (2005) *Trends Immunol* 26:565–571.
23. Zhang J, Cross AH, McCarthy TJ, Welch MJ (1997) *Nitric Oxide* 1:263–267.
24. Vowinckel E, Reutens D, Becher B, Verge G, Evans A, Owens T, Antel JP (1997) *J Neurosci Res* 50:345–353.
25. Versijpt J, Debruyne JC, Van Laere KJ, De Vos F, Keppens J, Strijckmans K, Achten E, Slegers G, Dierckx RA, Korf J, De Reuck JL (2005) *Mult Scler* 11:127–134.
26. Debruyne JC, Versijpt J, Van Laere KJ, De Vos F, Keppens J, Strijckmans K, Achten E, Slegers G, Dierckx RA, Korf J, De Reuck JL (2003) *Eur J Neurol* 10:257–264.
27. Stankoff B, Wang Y, Bottlaender M, Aigrot MS, Dolle F, Wu C, Feinstein D, Huang GF, Semah F, Mathis CA, *et al*. (2006) *Proc Natl Acad Sci USA* 103:9304–9309.
28. Mendel I, Kerlero de Rosbo N, Ben-Nun A (1995) *Eur J Immunol* 25:1951–1959.
29. Racke MK, Hu W, Lovett-Racke AE (2005) *Trends Immunol* 26:289–291.
30. Kerfoot SM, Long EM, Hickey MJ, Andonegui G, Lapointe BM, Zanardo RC, Bonder C, James WG, Robbins SM, Kubes P (2004) *J Immunol* 173:7070–7077.
31. Chow PL, Stout DB, Komisopoulou E, Chatziioannou AF (2006) *Phys Med Biol* 51:379–390.
32. Loening AM, Gambhir SS (2003) *Mol Imaging* 2:131–137.
33. Gallagher BM, Fowler JS, Gutterson NI, MacGregor RR, Wan CN, Wolf AP (1978) *J Nucl Med* 19:1154–1161.
34. DiRocco RJ, Hashim GA (1983) *Neurosci Lett* 37:105–110.
35. McKay LI, Cidlowski JA (1999) *Endocr Rev* 20:435–459.
36. Agnello D, Carvelli L, Muzio V, Villa P, Bottazzi B, Polentarutti N, Mennini T, Mantovani A, Ghezzi P (2000) *J Neuroimmunol* 109:105–111.
37. Krishnamoorthy G, Lassmann H, Wekerle H, Holz A (2006) *J Clin Invest* 116:2385–2392.
38. Bettelli E, Baeten D, Jager A, Sobel RA, Kuchroo VK (2006) *J Clin Invest* 116:2393–2402.
39. Bakshi R, Miletich RS, Kinkel PR, Emmet ML, Kinkel WR (1998) *J Neuroimaging* 8:228–234.
40. Pozzilli C, Fieschi C, Perani D, Paulesu E, Comi G, Bastianello S, Bernardi S, Bettinardi V, Bozzao L, Canal N, *et al*. (1992) *J Neurol Sci* 112:51–57.
41. Blinkenberg M, Jensen CV, Holm S, Paulson OB, Sorensen PS (1999) *Neurology* 53:149–153.
42. Blinkenberg M, Rune K, Jensen CV, Ravnborg M, Kyllingsbaek S, Holm S, Paulson OB, Sorensen PS (2000) *Neurology* 54:558–564.
43. Derache N, Marie RM, Constans JM, Defer GL (2006) *J Neurol Sci* 245:103–109.
44. Paulesu E, Perani D, Fazio F, Comi G, Pozzilli C, Martinelli V, Filippi M, Bettinardi V, Sirabian G, Passafiume D (1996) *NeuroImage* 4:87–96.
45. Sun X, Tanaka M, Kondo S, Okamoto K, Hirai S (1998) *Ann Nucl Med* 12:89–94.
46. Kutzelnigg A, Lucchinetti CF, Stadelmann C, Bruck W, Rauschka H, Bergmann M, Schmidbauer M, Parisi JE, Lassmann H (2005) *Brain* 128:2705–2712.
47. Tench CR, Morgan PS, Jaspan T, Auer DP, Constantinescu CS (2005) *J Neuroimaging* 15:94S–102S.
48. Gottesdiener KM, Karpinski BA, Lindsten T, Strominger JL, Jones NH, Thompson CB, Leiden JM (1988) *Mol Cell Biol* 8:3809–3819.
49. Qi J, Leahy RM, Cherry SR, Chatziioannou A, Farquhar TH (1998) *Phys Med Biol* 43:1001–1013.